

Supporting Information

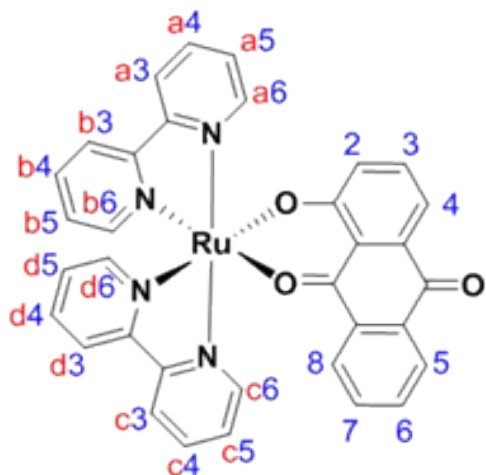
Hydrogen Peroxide Assisted Photorelease of an Anthraquinone-based Ligand from [Ru(2,2'-bipyridine)2(9,10-dioxo-9,10-dihydroanthracen-1-olate)]Cl in Aqueous Solution

L. Zeng, D. Sirbu, P. G. Waddell, N. V. Tkachenko, M. R. Probert and A. C. Benniston

Table of Contents

Figure S1. A 700 MHz ^1H NMR spectrum for Λ -RU1 in acetonitrile- d_3	3
Figure S2. A 175 MHz ^{13}C NMR spectrum for Λ -RU1 in acetonitrile- d_3	4
Figure S3. A COSY spectrum for Λ -RU1 in acetonitrile- d_3	4
Figure S4. A HSQC spectrum for Λ -RU1 in acetonitrile- d_3	5
Figure S5. A 700 MHz ^1H NMR spectrum for Δ -RU1 in acetonitrile- d_3	5
Figure S6. A 175 MHz ^{13}C NMR spectrum for Δ -RU1 in acetonitrile- d_3	6
Figure S7. A COSY spectrum for Δ -RU1 in acetonitrile- d_3	6
Figure S8. A HSQC spectrum for Δ -RU1 in acetonitrile- d_3	7
Figure S9. Observed and theoretical mass spectra for RU1 in $[\text{M}-\text{PF}_6]^+$ mode.	7
Table S1. Crystal structure determination of: RU1 ($\text{C}_{34}\text{H}_{23}\text{F}_6\text{N}_4\text{O}_3\text{PRu}$).....	8
Figure S10. CD spectra of enantiomers of Λ and Δ -RU1 dissolved in CH_3CN (a) or H_2O (b). The black and red curves represent the Λ and Δ isomers in the optical resolution respectively.....	15
Control Experiments.	16
Figure S11. Control experiments for RU1 under different conditions.....	17
Figure S12. Normalized UV-Vis absorption spectra of RU1 in pH 2 to pH 13 aqueous solutions.....	18
Figure S13. UV-Vis spectra of $[\text{Ru}(\text{bipy})_3](\text{PF}_6)_2$ in H_2O when treated with H_2O_2 in (a) kept in dark; (b) exposed to white light.....	19
Figure S14. Degradation of RU1 in the presence of H_2O_2 in an aqueous buffer solution from pH 2 to 13. The solution was deoxygenated with N_2 in advance of the measurements.....	21
Figure S15. Concentration of RU1 versus time at 580 nm in different pH conditions.....	23
Figure S16. Electrospray mass spectrum of an irradiated solution of RU1 in H_2O containing H_2O_2 and peak assignments.....	24
Figure S17. Partial ^1H NMR spectrum of pure 1-hydroxyanthra-9,10-quinone in CDCl_3 (A) and a partial ^1H NMR spectrum of a sample of RU1 in D_2O containing H_2O_2 after irradiation with white light (B). Highlighted peak represents proton shifted because of the presence of a paramagnetic ion.....	25

Figure S18. Normalised absorption spectrum of $[\text{Ru}(\text{bipy})_3](\text{PF}_6)_2$ in H_2O (black) and after oxidation with PbO_2 (red).....	26
Figure S19. Normalised absorption spectrum of RU1 in H_2O (pH 2) after irradiation for 70 mins in the presence of H_2O_2 (black) and the spectrum after the oxidation of RU1 with PbO_2 (red).....	27
DFT Calculation Results	28
Figure S20. Selection of DFT calculated Kohn-Sham frontier molecular orbitals for a gas-phase energy minimised structure of RU1 using Gaussian 09 and B3LYP with a split basis set with 3-21G* for Ru and 6-311G for all other atoms.....	29
Table S2. Calculated parameters from TD-DFT for energy minimised structure of RU1 in the gas phase using B3LYP and 3-21G* (Ru) and 6-311G (other atoms).....	30
Figure S21. Comparison of recorded normalized absorption spectrum of RU1 in MeCN (red) with calculated spectrum (black) for the energy minimized gas phase structure. The half-width for the calculated spectrum was set to 1100 cm^{-1} to match the actual spectrum.....	31
Figure S22. Calculated structure of $[\text{Ru}^{3+}(\text{bipy})_2\text{AQ}]^{2+}$ and the tilt angle between planes created using the RuN_2O_2 unit (red) and the anthraquinone-based ligand (blue).....	32
Figure S23. Selection of DFT calculated Kohn-Sham frontier molecular orbitals for a gas-phase energy minimised structure of $[\text{Ru}(\text{III})(\text{bipy})_2\text{AQ}]^{2+}$ using Gaussian 09 and B3LYP with a split basis set with 3-21G* for Ru and 6-311G for all other atoms.....	33
Figure S24. Comparison of X-ray structure for RU1 with calculated ground-state and first-excited triplet state structures.....	34



Chemical formula for **RU1**

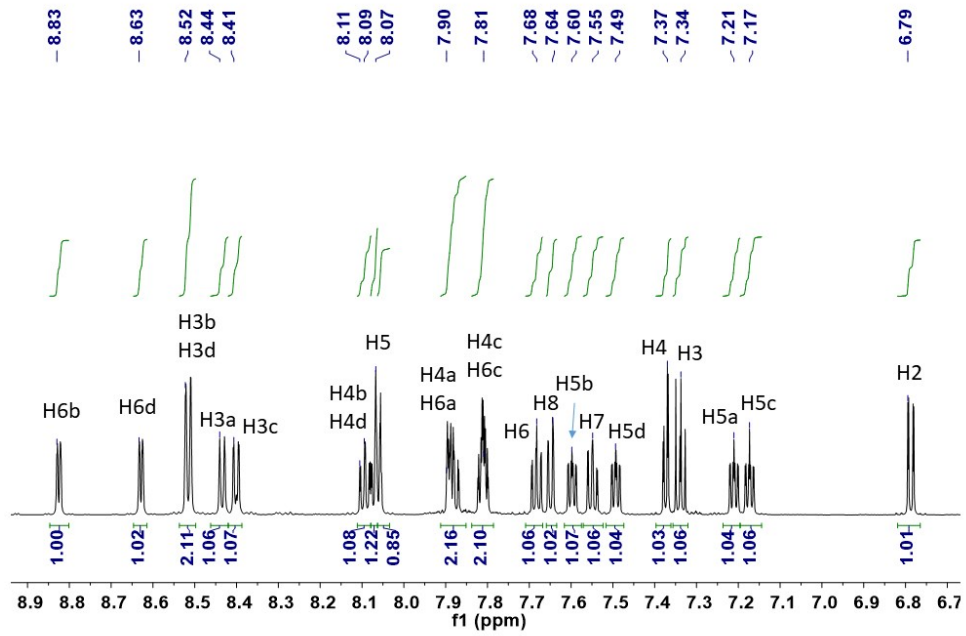


Figure S1. A 700 MHz ^1H NMR spectrum for Λ -**RU1** in acetonitrile- d_3 .

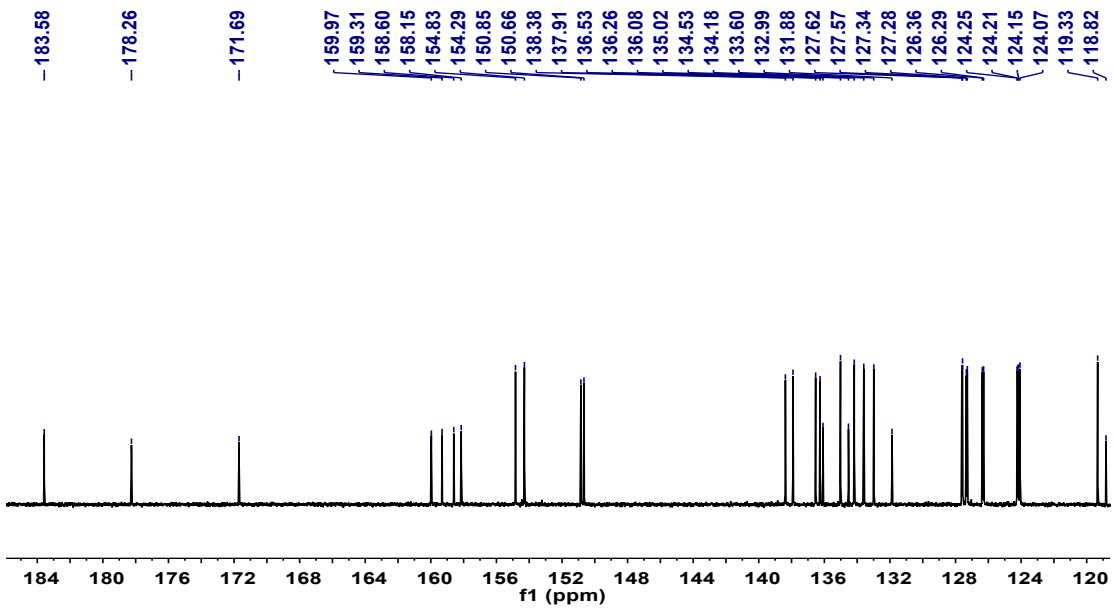


Figure S2. A 175MHz ^{13}C NMR spectrum for Λ -RU1 in acetonitrile- d_3 .

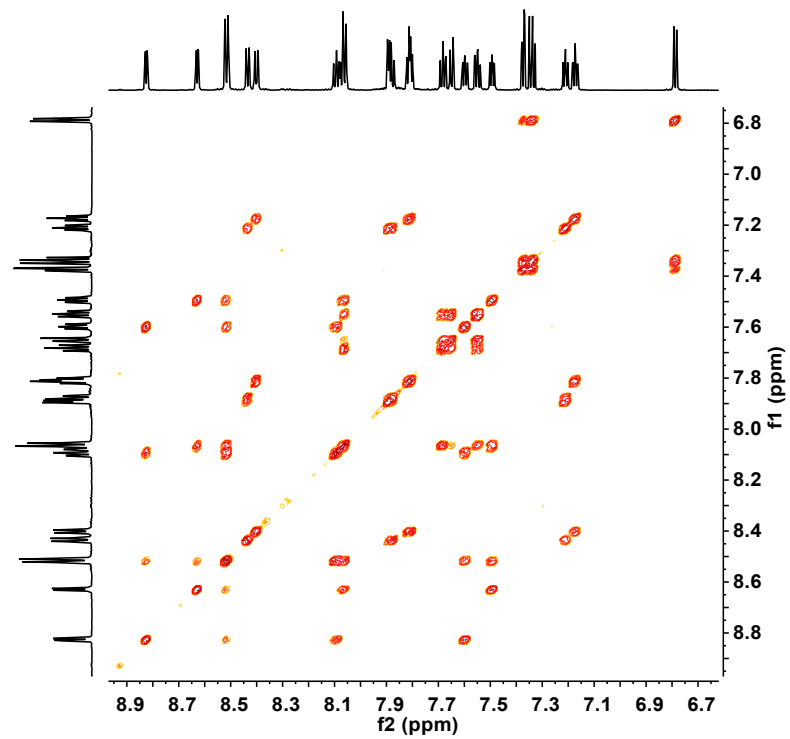


Figure S3. A COSY spectrum for Λ -RU1 in acetonitrile- d_3 .

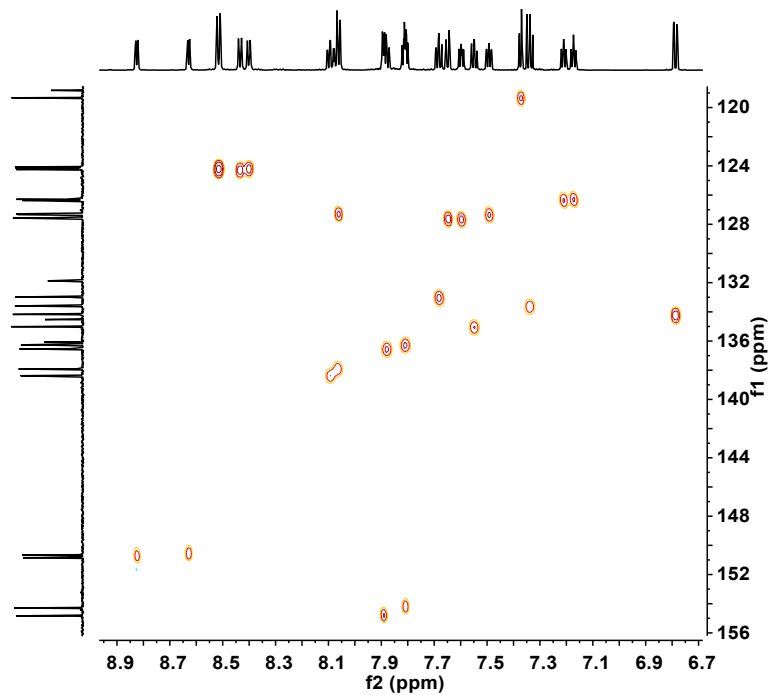


Figure S4. A HSQC spectrum for Δ -RU1 in acetonitrile- d_3 .

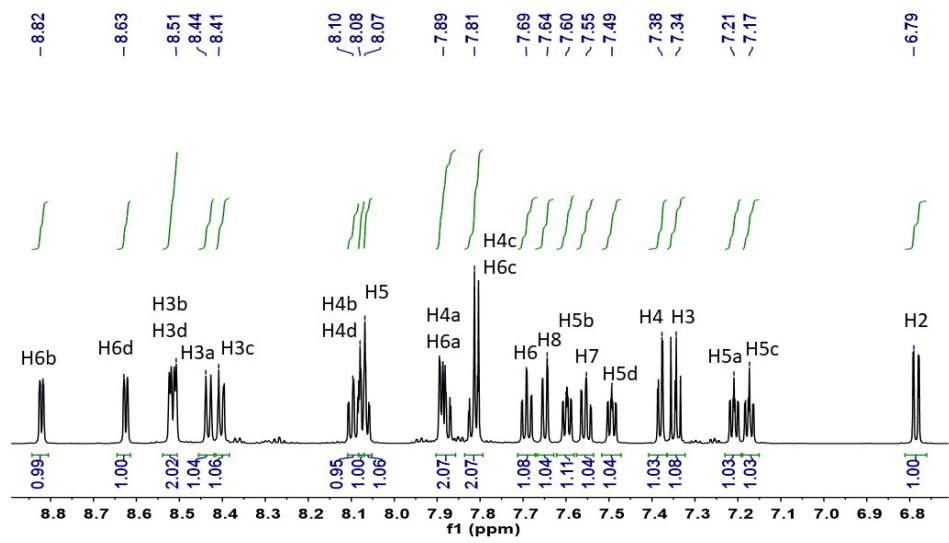


Figure S5. A 700 MHz ^1H NMR spectrum for Δ -RU1 in acetonitrile- d_3 .

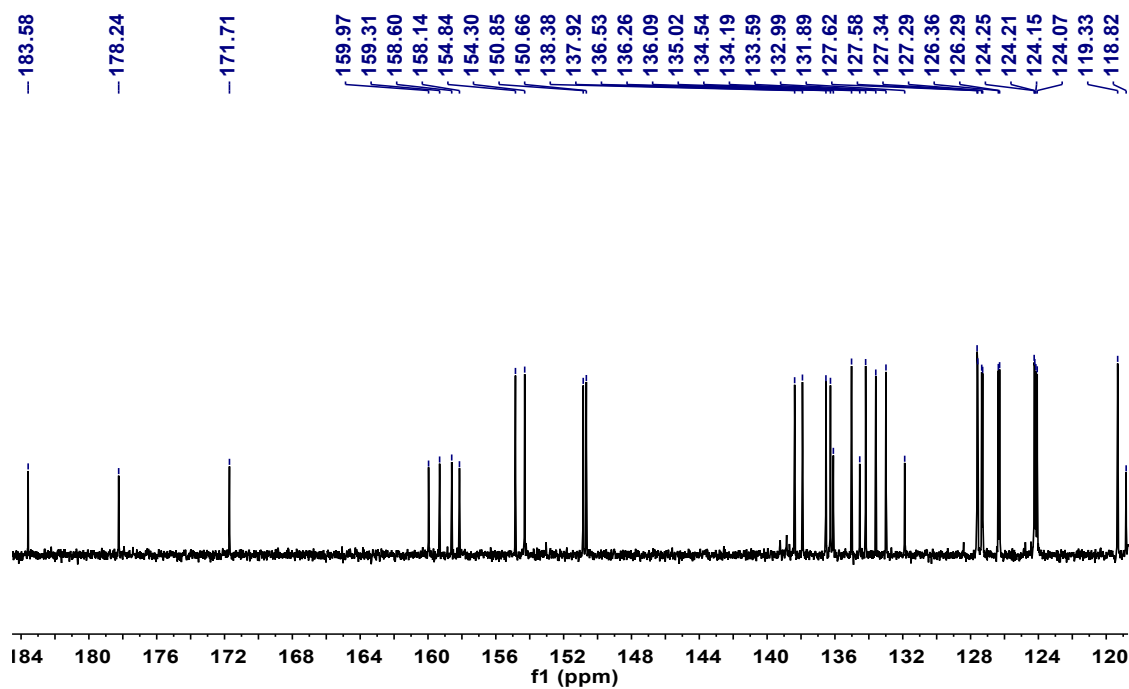


Figure S6. A 175 MHz ^{13}C NMR spectrum for $\Delta\text{-RU1}$ in acetonitrile- d_3 .

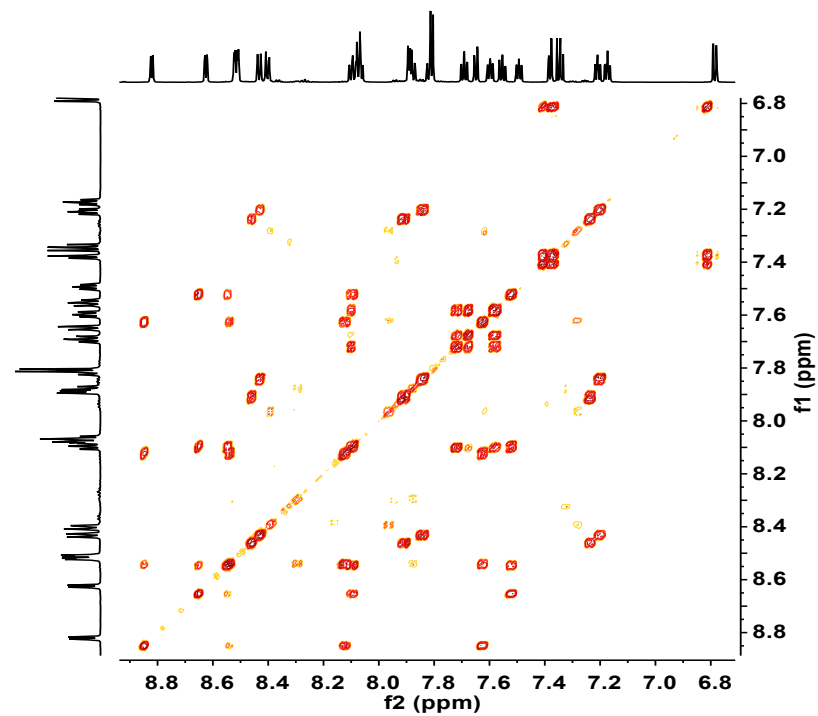


Figure S7. A COSY spectrum for $\Delta\text{-RU1}$ in acetonitrile- d_3 .

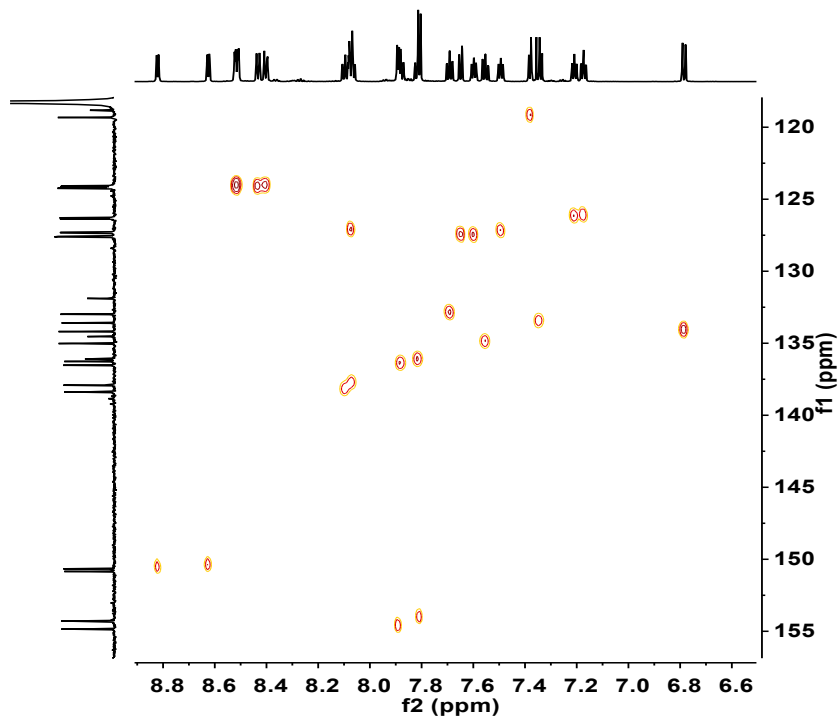
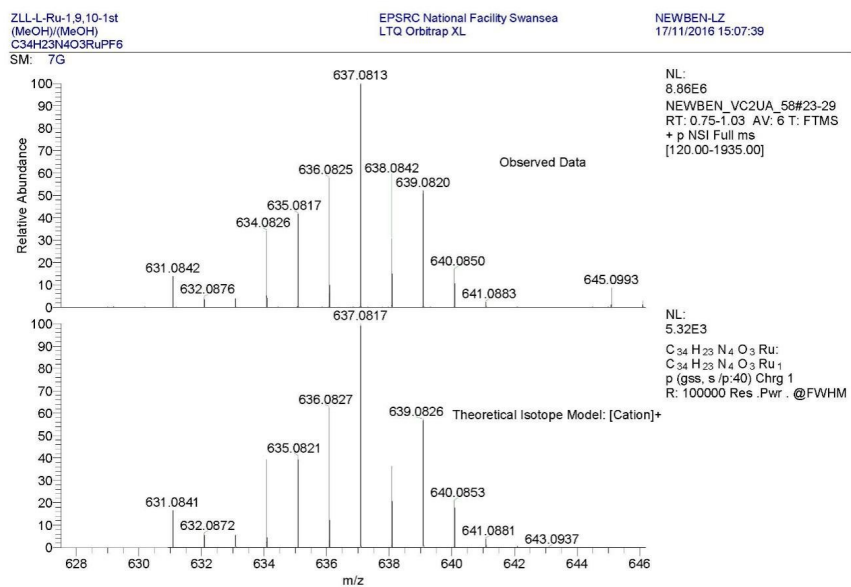


Figure S8. A HSQC spectrum for Δ -RU1 in acetonitrile- d_3 .



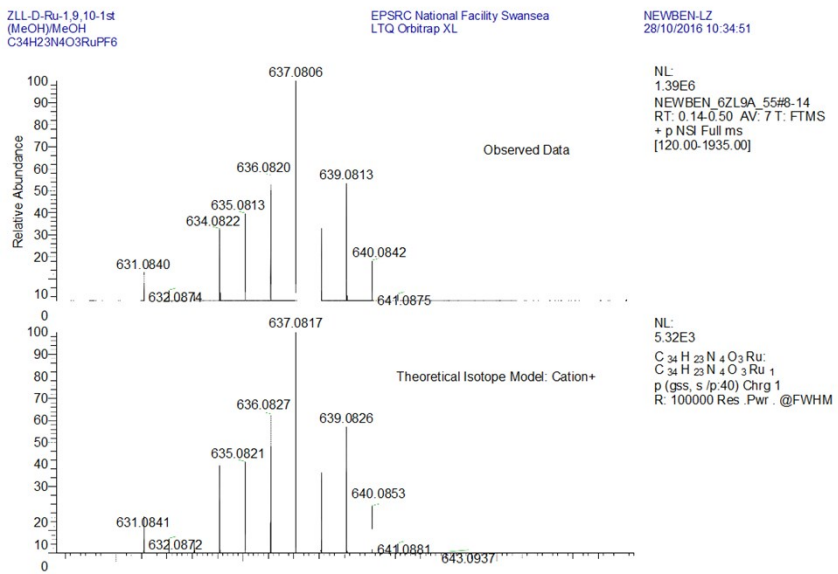


Figure S9. Observed and theoretical mass spectra for **RU1** in [M-PF₆]⁺ mode. Top: Lambda isomer and bottom: Delta isomer.

Table S1. Crystal structure determination of: **RU1** (C₃₄H₂₃F₆N₄O₃PRu)

Identification code	RU1
Empirical formula	C ₃₄ H ₂₃ F ₆ N ₄ O ₃ PRu
Formula weight	781.60
Temperature/K	100.0(2)
Crystal system	triclinic
Space group	P-1
a/Å	7.610(2)
b/Å	13.099(4)
c/Å	19.064(6)
α/°	101.261(5)
β/°	96.918(5)
γ/°	96.300(5)
Volume/Å ³	1832.9(10)
Z	2

ρ_{calc} g/cm ³	1.416
μ/mm^{-1}	0.535
F(000)	784.0
Crystal size/mm ³	0.04 × 0.013 × 0.007
Radiation	Synchrotron ($\lambda = 0.6889$)
2 Θ range for data collection/°	3.102 to 51.004
Index ranges	-9 ≤ h ≤ 9, -16 ≤ k ≤ 16, -23 ≤ l ≤ 23
Reflections collected	16741
Independent reflections	7290 [R _{int} = 0.0627, R _{sigma} = 0.1183]
Data/restraints/parameters	7290/471/442
Goodness-of-fit on F ²	1.088
Final R indexes [I >= 2σ(I)]	R ₁ = 0.0788, wR ₂ = 0.2087
Final R indexes [all data]	R ₁ = 0.1000, wR ₂ = 0.2228
Largest diff. peak/hole / e Å ⁻³	1.73/-0.55

Fractional Atomic Coordinates ($\times 10^4$) and Equivalent Isotropic Displacement Parameters (Å $^2 \times 10^3$) for acb180014. U_{eq} is defined as 1/3 of the trace of the orthogonalised U_{ij} tensor.

Atom	x	y	z	U(eq)
Ru1	5978.4(6)	7318.2(4)	2571.3(2)	46.7(2)
P1	8304(3)	1585.7(15)	1016.6(11)	72.2(5)
F1	8980(13)	2471(5)	1704(3)	149(3)
F2	6325(11)	1865(6)	1010(4)	141(2)
F3	8712(10)	2392(4)	515(3)	123(2)
F4	7637(8)	707(4)	328(2)	97.9(15)
F5	10290(8)	1317(5)	1006(4)	117.8(18)
F6	7987(7)	769(4)	1521(2)	84.7(13)
O1	7362(5)	8755(3)	3055.9(19)	42.7(8)
O2	5165(5)	7197(3)	3543(2)	51.3(9)
O3	8516(6)	11073(3)	5777(2)	61.3(11)
N1	4692(7)	5849(4)	2099(3)	59.1(12)
N2	7910(7)	6414(4)	2806(3)	53.1(11)
N3	6642(7)	7545(4)	1603(3)	54.6(12)

N4	4024(6)	8159(4)	2268(3)	49.6(11)
C1	7407(7)	9278(4)	3703(3)	43.3(11)
C2	5659(7)	7853(5)	4158(3)	47.5(12)
C3	5055(9)	7528(6)	4773(3)	60.1(15)
C4	5443(9)	8155(6)	5443(4)	62.2(16)
C5	6445(8)	9139(5)	5556(3)	51.7(13)
C6	8095(8)	10561(5)	5147(3)	49.0(12)
C7	9450(9)	12055(5)	4648(3)	57.4(15)
C8	9850(10)	12464(5)	4074(4)	62.2(16)
C9	9441(10)	11858(5)	3377(4)	63.6(17)
C10	8639(9)	10826(5)	3250(3)	54.8(14)
C11	6695(7)	8868(4)	4267(3)	44.5(11)
C12	7062(8)	9502(5)	4994(3)	46.4(12)
C13	8627(7)	11008(4)	4537(3)	44.2(12)
C14	8245(7)	10392(4)	3829(3)	44.0(11)
C15	5671(11)	5050(6)	2153(4)	75.0(19)
C16	4868(15)	4040(7)	1825(7)	120(4)
C17	3197(16)	3808(9)	1485(7)	127(4)
C18	2248(13)	4588(7)	1455(5)	95(3)
C19	3003(10)	5610(7)	1752(4)	76(2)
C20	7475(10)	5358(5)	2548(4)	67.0(16)
C21	8706(13)	4670(6)	2667(5)	88(2)
C22	10332(13)	5051(7)	3048(6)	90(2)
C23	10785(11)	6117(6)	3320(5)	74.0(19)
C24	9541(8)	6768(5)	3199(3)	53.7(14)
C25	5649(9)	8183(5)	1274(3)	59.5(14)
C26	6056(12)	8450(6)	658(4)	73.0(18)
C27	7483(12)	8122(6)	346(4)	76.5(19)
C28	8425(11)	7453(6)	654(4)	74.5(18)
C29	7997(9)	7174(6)	1285(4)	65.6(17)
C30	4130(9)	8522(5)	1649(4)	59.6(15)
C31	2907(12)	9126(7)	1405(5)	82(2)
C32	1526(12)	9374(7)	1812(4)	81(2)
C33	1454(10)	9037(6)	2444(4)	67.7(17)
C34	2729(8)	8462(5)	2667(4)	55.6(14)

Anisotropic Displacement Parameters ($\text{\AA}^2 \times 10^3$) for acb180014. The Anisotropic displacement factor exponent takes the form: $-2\pi^2[h^2a^{*2}U_{11} + 2hka^{*}b^{*}U_{12} + \dots]$.

Atom	U_{11}	U_{22}	U_{33}	U_{23}	U_{13}	U_{12}
Ru1	33.8(3)	55.8(3)	43.5(3)	-2.54(19)	2.18(18)	2.82(18)

P1	95.4(15)	58.6(10)	66.2(12)	16.2(8)	19.6(10)	13.0(10)
F1	250(8)	85(3)	102(4)	4(3)	13(4)	20(4)
F2	157(5)	169(6)	123(5)	51(4)	47(4)	76(4)
F3	191(6)	80(3)	116(4)	45(3)	45(4)	24(3)
F4	146(5)	83(3)	66(3)	25(2)	8(3)	15(3)
F5	99(4)	130(4)	140(5)	58(4)	33(3)	12(3)
F6	103(4)	89(3)	69(3)	30(2)	19(2)	12(2)
O1	33.4(19)	52(2)	40.2(19)	3.4(15)	5.0(15)	6.7(15)
O2	41(2)	61(2)	47(2)	4.4(17)	7.5(17)	-1.0(17)
O3	67(3)	67(3)	41(2)	-1.1(18)	7(2)	-7(2)
N1	46(3)	73(3)	43(3)	-11(2)	-5(2)	-3(2)
N2	39(2)	60(3)	55(3)	1(2)	7(2)	5.6(19)
N3	52(3)	59(3)	47(3)	-3(2)	8(2)	5(2)
N4	39(2)	57(3)	49(2)	3(2)	3.2(19)	4.7(19)
C1	30(3)	49(3)	48(3)	3(2)	7(2)	9(2)
C2	30(3)	61(3)	48(3)	8(2)	0(2)	3(2)
C3	46(3)	77(4)	54(3)	14(3)	7(3)	-4(3)
C4	51(4)	80(4)	52(3)	14(3)	10(3)	-6(3)
C5	41(3)	70(3)	43(3)	10(2)	8(2)	5(2)
C6	39(3)	59(3)	45(3)	3(2)	6(2)	5(2)
C7	57(4)	58(3)	50(3)	0(2)	6(3)	1(3)
C8	69(4)	52(3)	64(3)	8(3)	16(3)	4(3)
C9	81(5)	56(3)	57(3)	15(3)	20(3)	8(3)
C10	60(4)	57(3)	51(3)	8(2)	16(3)	18(3)
C11	33(3)	58(3)	40(2)	7(2)	3(2)	8(2)
C12	37(3)	57(3)	43(3)	6(2)	4(2)	6(2)
C13	37(3)	47(3)	47(3)	2(2)	10(2)	9(2)
C14	34(3)	51(3)	47(3)	4(2)	9(2)	9(2)
C15	69(4)	67(4)	78(5)	-9(3)	8(3)	7(3)
C16	97(6)	72(4)	154(9)	-44(5)	-4(5)	-5(4)
C17	104(6)	94(5)	144(9)	-39(5)	-6(6)	-17(4)
C18	80(5)	99(5)	78(5)	-19(4)	0(4)	-25(4)
C19	55(4)	96(4)	58(4)	-14(3)	-2(3)	-11(3)
C20	65(3)	56(3)	73(4)	-5(3)	14(3)	6(2)
C21	86(5)	61(4)	113(6)	5(4)	15(4)	22(3)
C22	79(5)	73(4)	121(7)	23(4)	13(4)	27(3)
C23	55(4)	77(4)	93(5)	27(4)	6(3)	14(3)
C24	41(3)	57(3)	63(4)	14(3)	8(2)	4(2)
C25	58(3)	63(3)	50(3)	1(2)	4(3)	1(3)
C26	88(5)	71(4)	56(4)	7(3)	13(3)	2(3)
C27	91(5)	72(4)	63(4)	4(3)	28(4)	-4(3)
C28	73(5)	81(4)	62(4)	-7(3)	25(3)	0(3)

C29	53(4)	82(4)	55(3)	-5(3)	14(3)	6(3)
C30	57(3)	65(4)	54(3)	9(3)	7(3)	4(3)
C31	92(5)	96(5)	74(4)	37(4)	22(4)	35(4)
C32	71(5)	100(6)	80(4)	28(4)	12(4)	37(4)
C33	54(4)	85(5)	68(4)	18(3)	10(3)	22(3)
C34	36(3)	67(4)	62(3)	9(3)	8(3)	3(2)

Bond Lengths for acb180014.

Atom	Atom	Length/ \AA	Atom	Atom	Length/ \AA
Ru1	O1	2.038(4)	C5	C12	1.366(8)
Ru1	O2	2.052(4)	C6	C12	1.475(8)
Ru1	N1	2.043(5)	C6	C13	1.480(8)
Ru1	N2	2.048(5)	C7	C8	1.361(9)
Ru1	N3	2.038(5)	C7	C13	1.409(8)
Ru1	N4	2.040(5)	C8	C9	1.388(9)
P1	F1	1.563(7)	C9	C10	1.384(9)
P1	F2	1.587(7)	C10	C14	1.384(8)
P1	F3	1.587(5)	C11	C12	1.448(8)
P1	F4	1.558(5)	C13	C14	1.409(8)
P1	F5	1.590(6)	C15	C16	1.386(11)
P1	F6	1.590(5)	C15	C20	1.457(11)
O1	C1	1.283(6)	C16	C17	1.331(15)
O2	C2	1.298(7)	C17	C18	1.319(15)
O3	C6	1.241(7)	C18	C19	1.379(11)
N1	C15	1.363(9)	C20	C21	1.399(11)
N1	C19	1.347(9)	C21	C22	1.347(13)
N2	C20	1.363(8)	C22	C23	1.380(11)
N2	C24	1.354(8)	C23	C24	1.370(9)
N3	C25	1.375(9)	C25	C26	1.350(10)
N3	C29	1.347(8)	C25	C30	1.495(9)
N4	C30	1.362(8)	C26	C27	1.369(11)
N4	C34	1.363(7)	C27	C28	1.365(12)
C1	C11	1.428(8)	C28	C29	1.388(10)
C1	C14	1.489(8)	C30	C31	1.382(10)
C2	C3	1.430(8)	C31	C32	1.408(11)
C2	C11	1.434(8)	C32	C33	1.367(11)
C3	C4	1.356(9)	C33	C34	1.369(9)
C4	C5	1.388(9)			

Bond Angles for acb180014.

Atom	Atom	Atom	Angle/ [°]	Atom	Atom	Atom	Angle/ [°]
O1	Ru1	O2	88.79(15)	C4	C3	C2	121.5(6)
O1	Ru1	N1	177.42(18)	C3	C4	C5	121.0(6)
O1	Ru1	N2	98.36(18)	C12	C5	C4	120.7(6)
O1	Ru1	N3	89.31(17)	O3	C6	C12	120.8(5)
O1	Ru1	N4	84.41(17)	O3	C6	C13	120.2(5)
N1	Ru1	O2	91.15(19)	C12	C6	C13	119.0(5)
N1	Ru1	N2	79.1(2)	C8	C7	C13	119.9(6)
N2	Ru1	O2	87.29(18)	C7	C8	C9	120.5(6)
N3	Ru1	O2	174.72(18)	C10	C9	C8	121.0(6)
N3	Ru1	N1	91.0(2)	C14	C10	C9	119.3(6)
N3	Ru1	N2	97.9(2)	C1	C11	C2	123.8(5)
N3	Ru1	N4	79.4(2)	C1	C11	C12	118.5(5)
N4	Ru1	O2	95.55(18)	C2	C11	C12	117.7(5)
N4	Ru1	N1	98.2(2)	C5	C12	C6	118.2(5)
N4	Ru1	N2	176.09(19)	C5	C12	C11	120.9(5)
F1	P1	F2	91.1(4)	C11	C12	C6	121.0(5)
F1	P1	F3	90.3(4)	C7	C13	C6	121.0(5)
F1	P1	F5	89.4(4)	C14	C13	C6	119.6(5)
F1	P1	F6	89.5(3)	C14	C13	C7	119.3(5)
F2	P1	F5	178.6(3)	C10	C14	C1	120.0(5)
F2	P1	F6	92.4(3)	C10	C14	C13	120.0(5)
F3	P1	F2	90.2(4)	C13	C14	C1	120.0(5)
F3	P1	F5	88.5(3)	N1	C15	C16	117.2(8)
F3	P1	F6	177.4(4)	N1	C15	C20	115.8(6)
F4	P1	F1	179.6(4)	C16	C15	C20	127.0(8)
F4	P1	F2	89.0(4)	C17	C16	C15	124.0(10)
F4	P1	F3	89.4(3)	C18	C17	C16	118.0(9)
F4	P1	F5	90.5(3)	C17	C18	C19	120.3(9)
F4	P1	F6	90.8(3)	N1	C19	C18	121.9(8)
F6	P1	F5	88.9(3)	N2	C20	C15	114.0(6)
C1	O1	Ru1	128.9(3)	N2	C20	C21	120.7(7)
C2	O2	Ru1	126.9(4)	C21	C20	C15	125.3(7)
C15	N1	Ru1	115.2(5)	C22	C21	C20	119.8(8)
C19	N1	Ru1	126.3(5)	C21	C22	C23	120.2(8)
C19	N1	C15	118.5(6)	C24	C23	C22	118.5(8)
C20	N2	Ru1	116.0(5)	N2	C24	C23	122.8(6)
C24	N2	Ru1	126.0(4)	N3	C25	C30	114.5(6)
C24	N2	C20	118.0(6)	C26	C25	N3	120.7(7)
C25	N3	Ru1	115.6(4)	C26	C25	C30	124.8(7)
C29	N3	Ru1	126.0(5)	C25	C26	C27	121.8(8)

C29	N3	C25	118.2(6)	C28	C27	C26	117.7(7)
C30	N4	Ru1	116.9(4)	C27	C28	C29	120.3(7)
C30	N4	C34	117.8(6)	N3	C29	C28	121.1(7)
C34	N4	Ru1	125.0(4)	N4	C30	C25	113.3(6)
O1	C1	C11	124.7(5)	N4	C30	C31	121.7(6)
O1	C1	C14	114.3(5)	C31	C30	C25	125.0(6)
C11	C1	C14	121.0(5)	C30	C31	C32	118.8(7)
O2	C2	C3	115.8(5)	C33	C32	C31	119.4(7)
O2	C2	C11	125.9(5)	C32	C33	C34	119.2(7)
C3	C2	C11	118.2(5)	N4	C34	C33	122.9(6)

Hydrogen Atom Coordinates ($\text{\AA} \times 10^4$) and Isotropic Displacement Parameters ($\text{\AA}^2 \times 10^3$) for acb180014.

Atom	x	y	z	U(eq)
H3	4368	6857	4710	72
H4	5022	7917	5840	75
H5	6704	9566	6030	62
H7	9726	12476	5124	69
H8	10413	13169	4150	75
H9	9715	12157	2980	76
H10	8363	10418	2771	66
H16	5554	3480	1843	144
H17	2701	3103	1270	153
H18	1040	4444	1228	114
H19	2311	6163	1710	92
H21	8397	3937	2479	105
H22	11171	4585	3129	108
H23	11932	6393	3586	89
H24	9836	7499	3400	64
H26	5332	8877	434	88
H27	7806	8351	-69	92
H28	9378	7177	435	89
H29	8672	6713	1496	79
H31	2996	9370	971	98
H32	652	9773	1648	97
H33	532	9198	2724	81
H34	2709	8266	3120	67

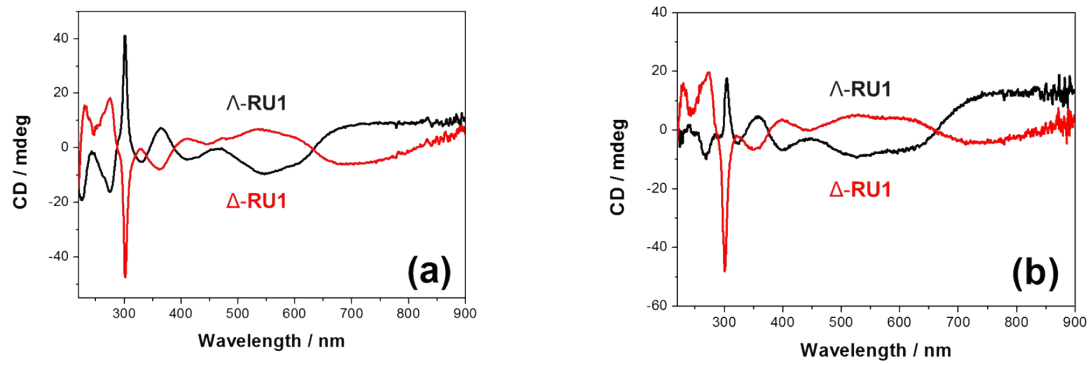


Figure S10. CD spectra of enantiomers of Λ and Δ -RU1 dissolved in CH₃CN **(a)** or H₂O **(b)**. The black and red curves represent the Λ and Δ isomers in the optical resolution respectively.

Control Experiments

To investigate the influence of H₂O₂, O₂ and light in the degradation reaction of **RU1**, several control experiments were carried out with different conditions in non-buffered H₂O solutions. All the H₂O₂ solutions were prepared in 0.3 M concentration. Without any H₂O₂, O₂ and light. **Figure S12 (a)** shows that **RU1** is stable in solution over 6 hours. By comparing **Figure S12 (b), (c) and (d)**, the degradation reaction only occurs in the presence of both H₂O₂ and light. **Figure S12 (e)** indicates that the ground state complex **RU1** can be oxidized with both O₂ and H₂O present. **Figure S12 (f)** shows that light drives the degradation reaction further with H₂O₂ and O₂ present in solution.

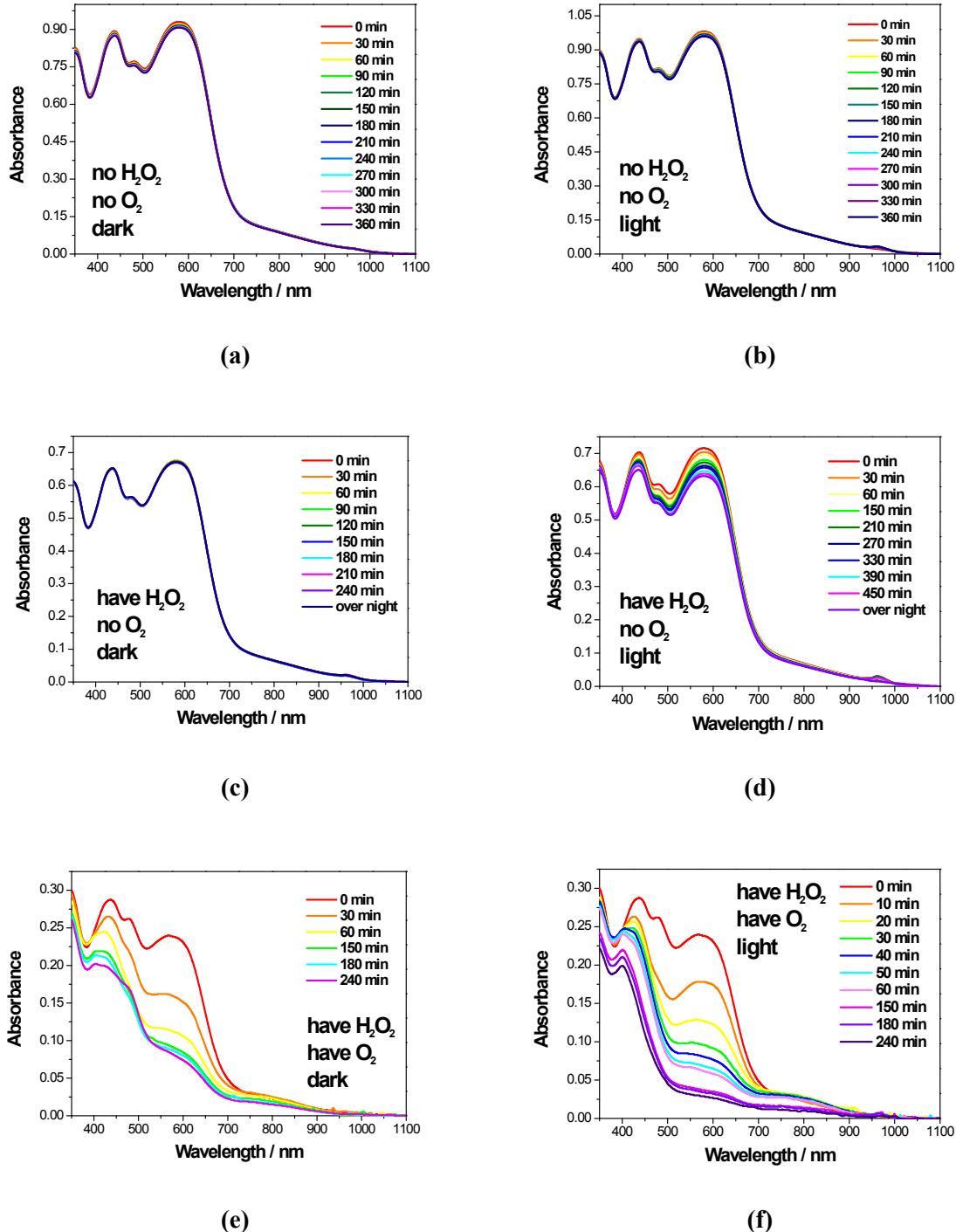


Figure S11. Control experiments for **RU1** under different conditions.

General Observations in Different pH Aqueous Solutions

UV-Vis absorption data were collected for **RU1** in an aqueous buffer solution ranging from pH 2 to 13. The spectra as a function of different pH are shown in **Figure S12**. As can be seen there is very little difference in the spectra over the whole pH range. In the ground state it would appear that the anthraquinone-based ligand is not protonated, at least down to a pH = 2, assuming that it would perturb the absorption spectrum. Under basic conditions there also appears to be no decomposition of the complex.

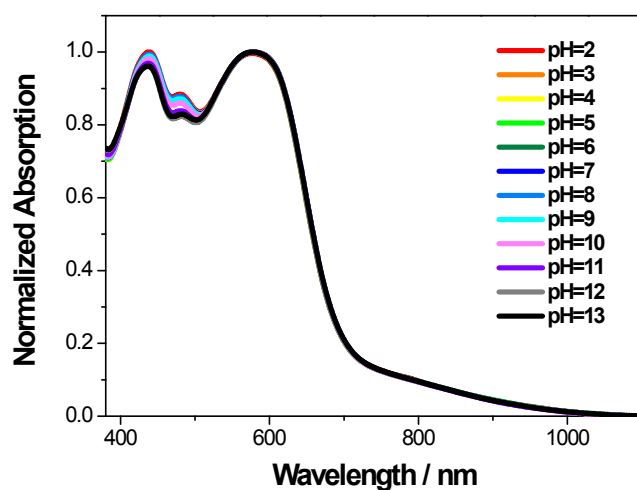


Figure S12. Normalized UV-Vis absorption spectra of **RU1** in pH 2 to pH 13 aqueous solutions.

[Ru(bipy)₃](PF₆)₂ with H₂O₂

[Ru(bipy)₃](PF₆)₂ in a deoxygenated H₂O solution was treated with H₂O₂ and exposed to light or kept in dark over 1 hour. During this hour UV-Vis spectra were recorded every 10 min. From **Figure S13** it is evident that the spectra remain identical throughout all the measurements as expected due to the stability of the complex.¹ This result indicates that any reaction of H₂O₂ with the ground and excited-state complex is very slow and unlikely to result in the dissociation of the bipyridine ligands.

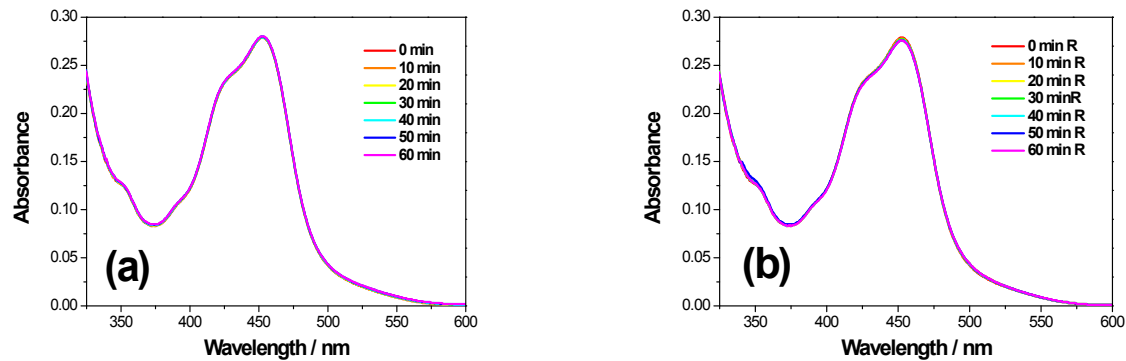
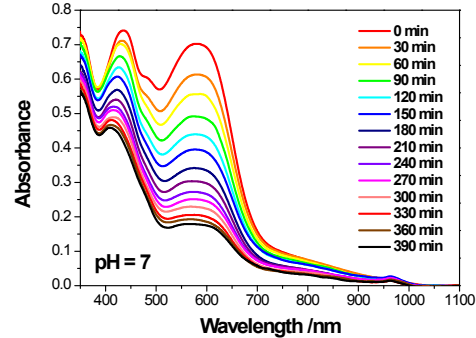
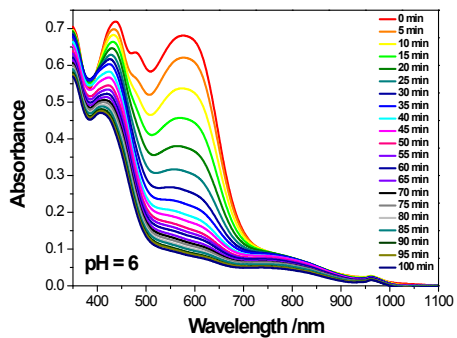
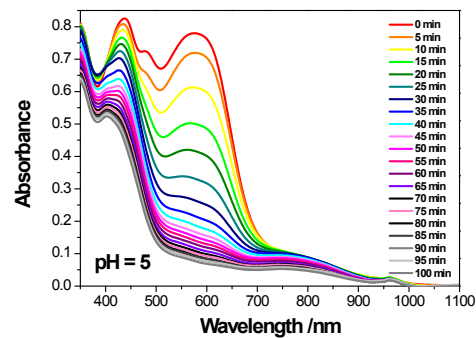
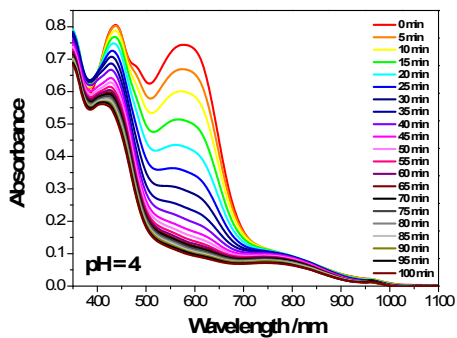
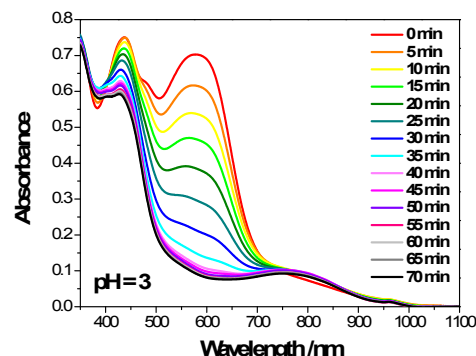
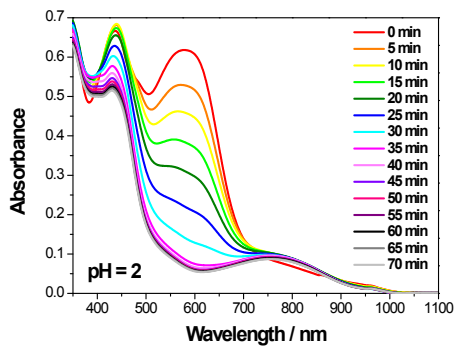


Figure S13. UV-Vis spectra of [Ru(bipy)₃](PF₆)₂ in H₂O when treated with H₂O₂ in **(a)** kept in dark; **(b)** exposed to white light.



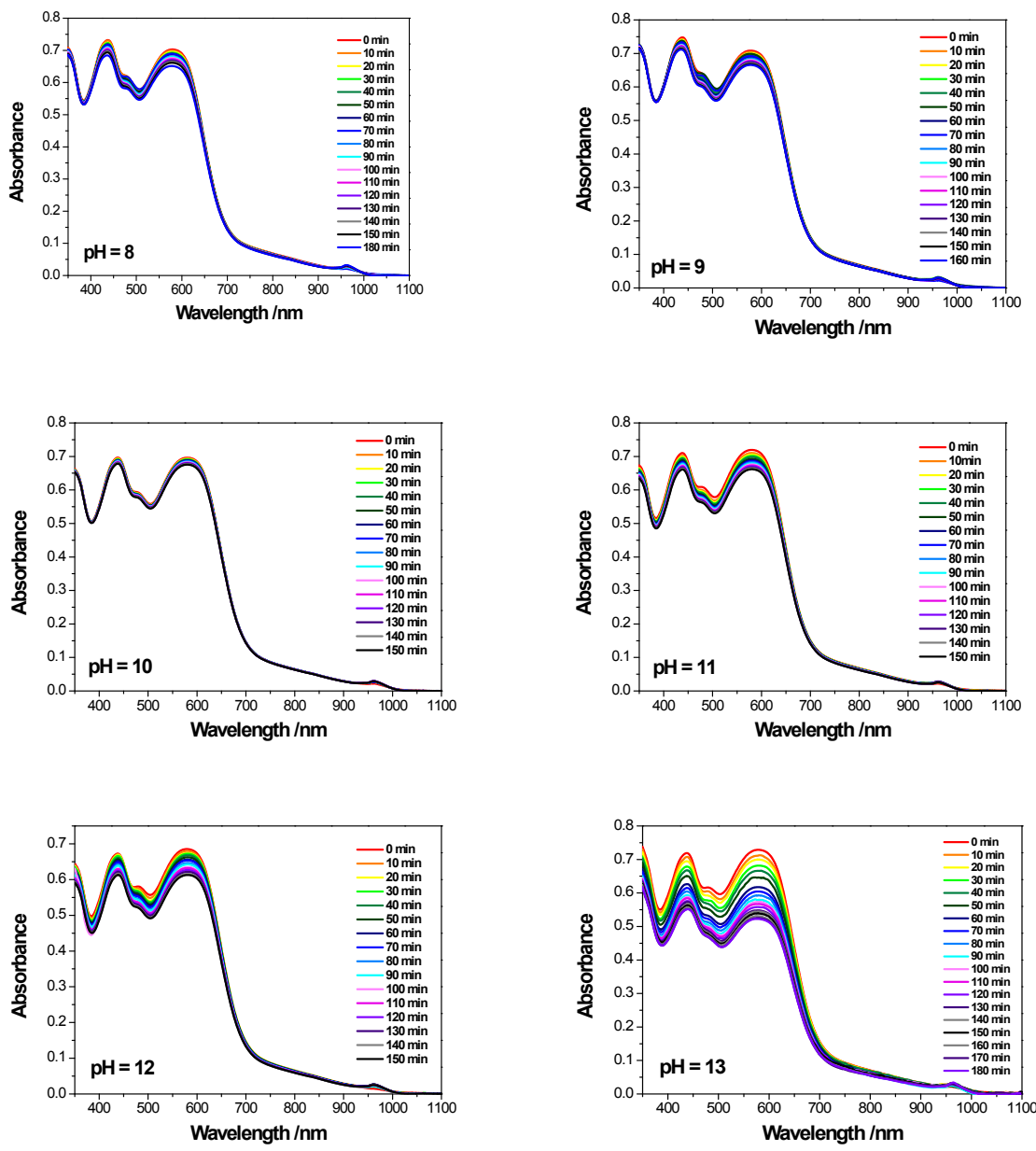
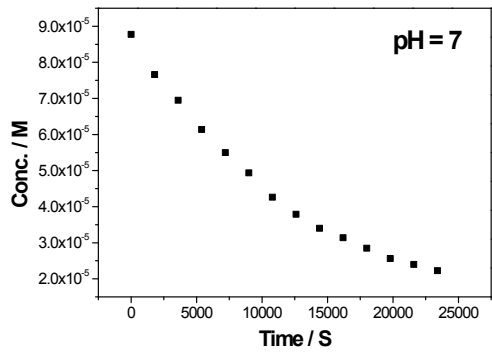
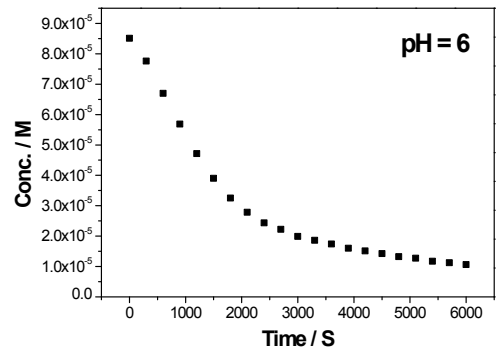
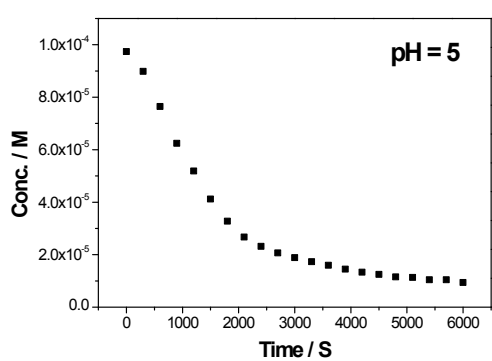
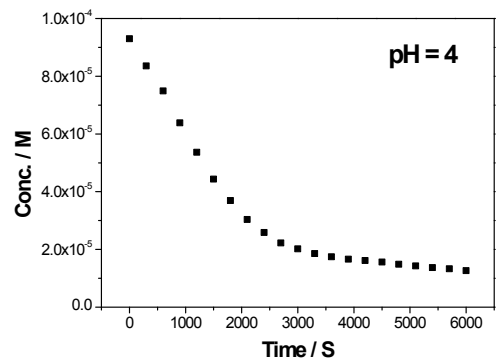
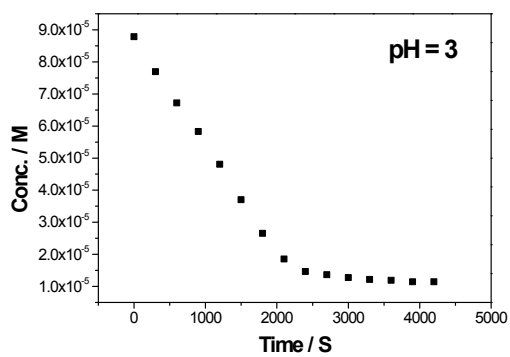
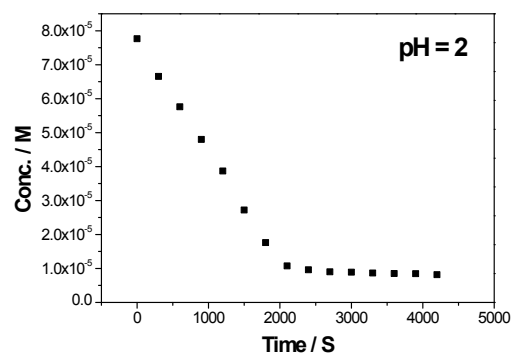


Figure S14. Degradation of RU1 in the presence of H₂O₂ in an aqueous buffer solution from pH 2 to 13. The solution was deoxygenated with N₂ in advance of the measurements.



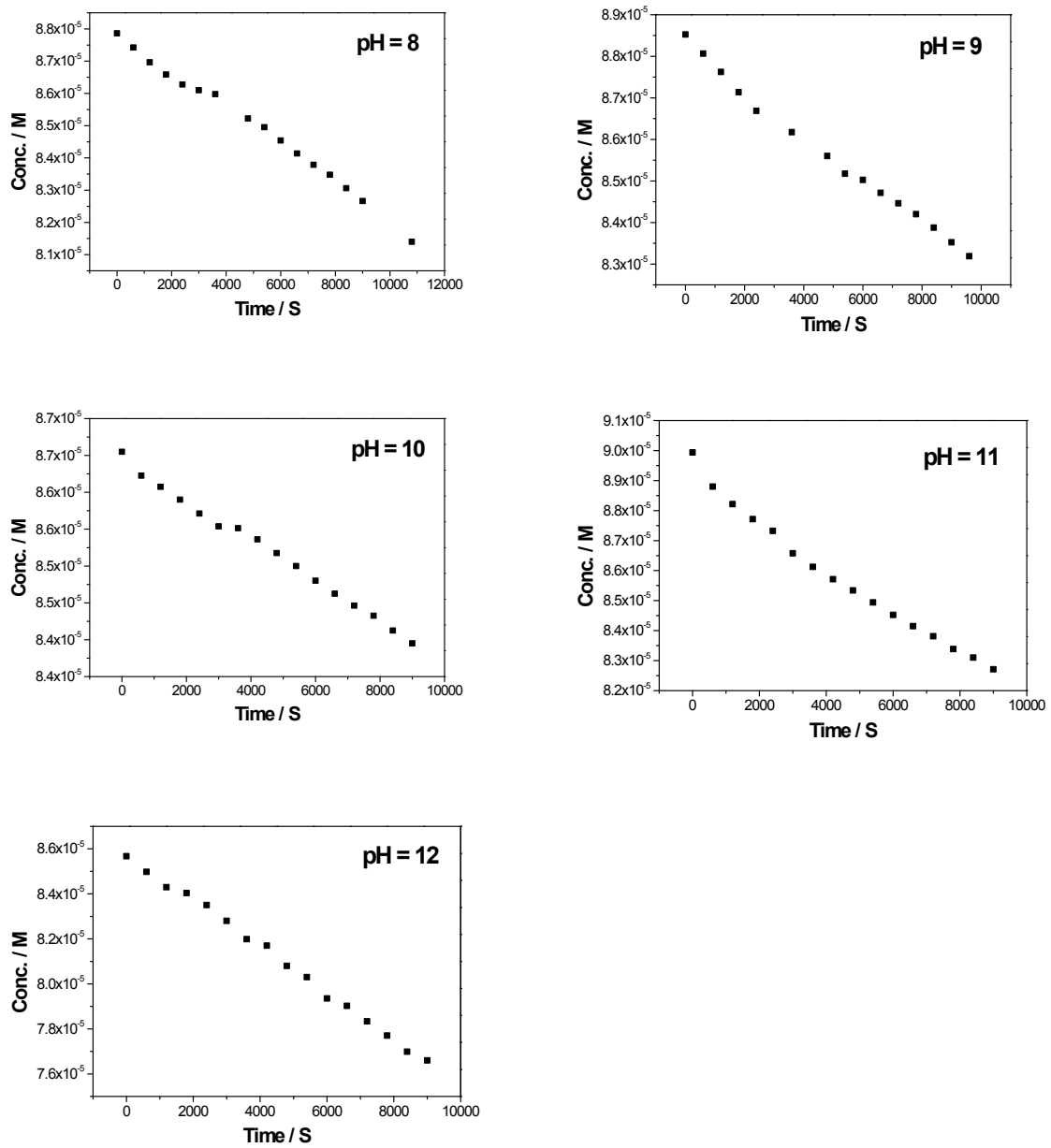


Figure S15. Concentration of RU1 versus time at 580 nm in different pH conditions.

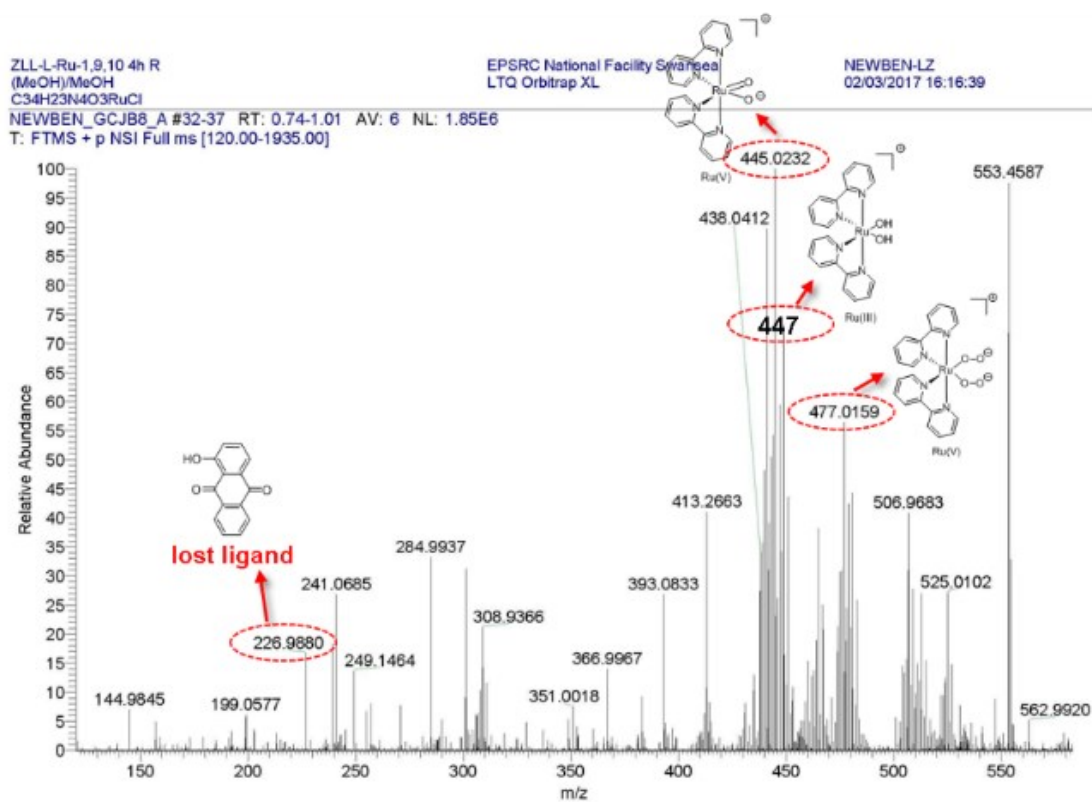


Figure S16. Electrospray mass spectrum of an irradiated solution of **RU1** in H₂O containing H₂O₂ and peak assignments.

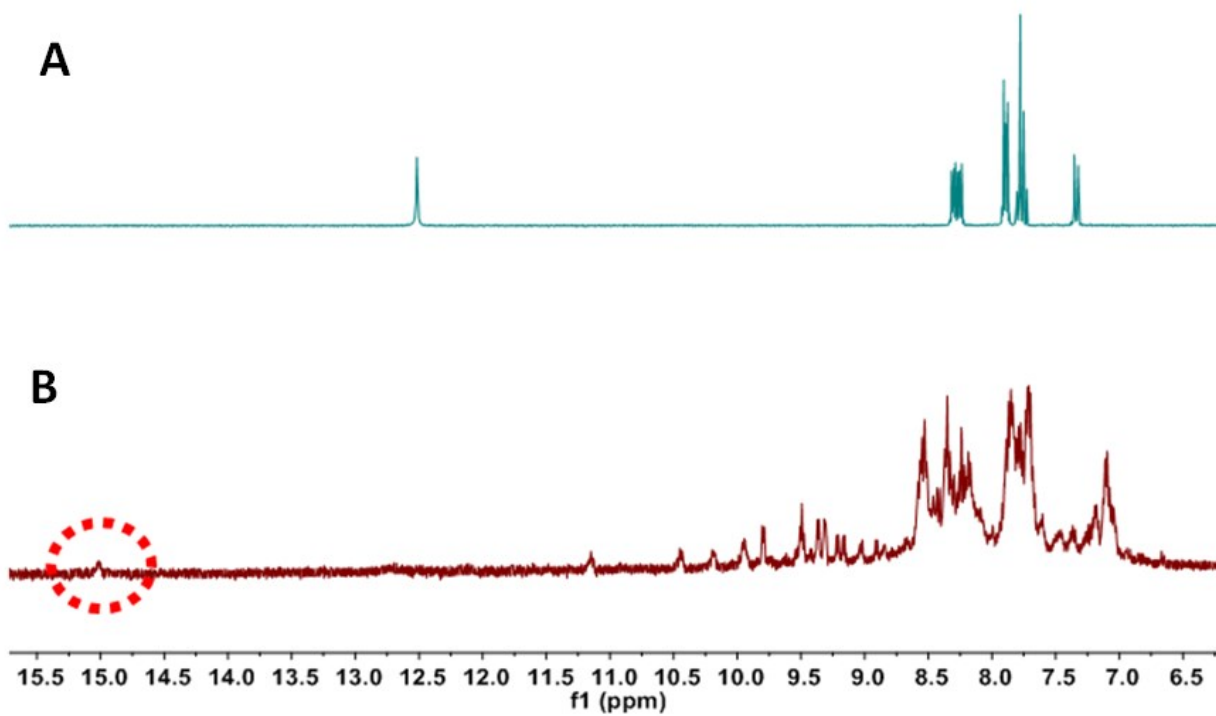


Figure S17. Partial ^1H NMR spectrum of pure 1-hydroxyanthra-9,10-quinone in CDCl_3 (**A**) and a partial ^1H NMR spectrum of a sample of **RU1** in D_2O containing H_2O_2 after irradiation with white light (**B**). Highlighted peak represents proton shifted because of the presence of a paramagnetic ion.

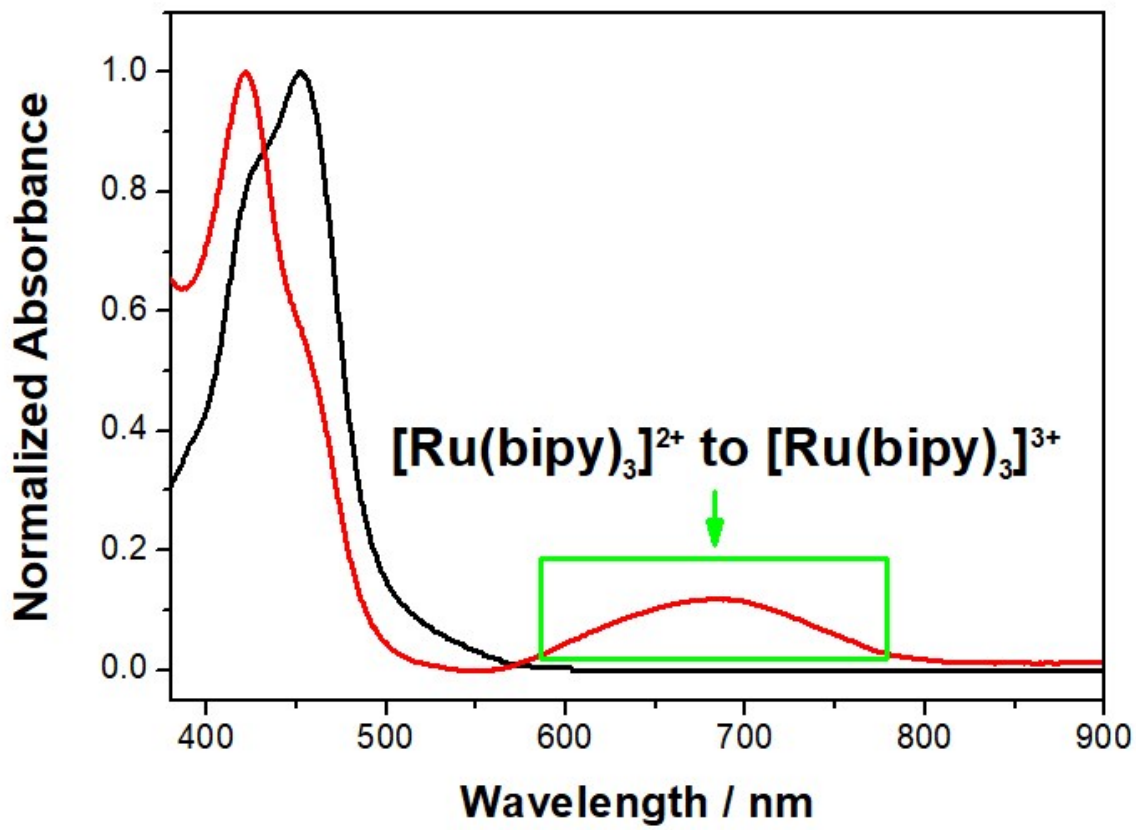


Figure S18. Normalised absorption spectrum of $[\text{Ru}(\text{bipy})_3](\text{PF}_6)_2$ in H_2O (black) and after oxidation with PbO_2 (red).

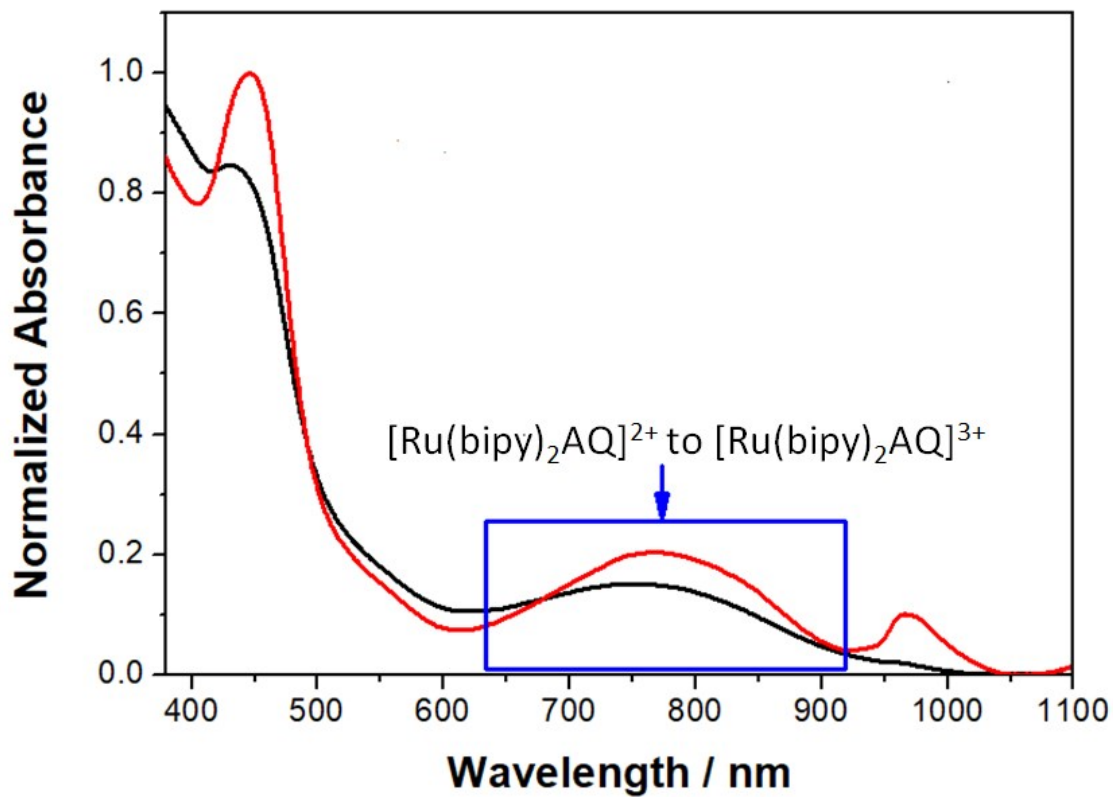


Figure S19. Normalised absorption spectrum of **RU1** in H₂O (pH 2) after irradiation for 70 mins in the presence of H₂O₂ (black) and the spectrum after the oxidation of **RU1** with PbO₂ (red).

DFT Calculation Results

A selection of the Kohn-Sham frontier molecular orbitals obtained for the energy minimized structure are shown in Figure S20. Unlike the case for $[\text{Ru}(\text{bipy})_3]^{2+}$ in which the HOMO is exclusively localised at the dz^2 orbital of the ruthenium ion, the HOMO for **[Ru(II)(bipy)₂AQ]⁺ (RU1)** is delocalised onto the anthraquinone-based ligand. The single d-orbital contribution from the ruthenium ion to the HOMO is from the t_{2g} set (dyz) and hence points in between the ligands. The HOMO-1 is far more clear-cut and is localised on the ruthenium ion and again is from the t_{2g} set (dxy). The LUMO is exclusively associated with the anthraquinone-based ligand, with LUMO+1 and LUMO+2 located at the bipyridine sites. A significant finding from the calculation relates to electron exchange between the HOMO-LUMO. In $[\text{Ru}(\text{bipy})_3]^{2+}$ the electronic transition is metal-to-ligand charge-transfer (MLCT), but the case for **RU1** is less evident and is best discussed in terms of a mixed MLCT/ $\pi-\pi^*$ electronic transition. To further this point a time-dependent DFT (TD-DFT) calculation performed on the ground-state structure of **RU1** elucidated the vertical Franck-Condon transitions. Collected in Table S2 is a summary of the findings and a calculated absorption spectrum is shown in Figure S21. The low-energy envelope to the absorption spectrum is dominated by HOMO to LUMO/LUMO+1 electronic transitions, and are consequently of mixed MLCT/ $\pi-\pi^*$ character. The high-energy side to the absorption envelope is mainly pure MLCT and is in fact similar to $[\text{Ru}(\text{bipy})_3]^{2+}$ since the electron accepting orbital is a bipyridine. For rigour purposes DFT calculations were also performed on **[Ru(III)(bipy)₂AQ]²⁺** which represents the oxidised version at the metal centre. Apart from small alterations in the Ru-N and Ru-O bond lengths, the most noteable feature of the energy-minimised structure is the distortion at the anthraquinone-based ligand site and its tilting out of the RuO_2N_2 plane by around *ca.* 13° (Figure S22). The modification of the Kohn-Sham molecular orbitals is significant and although the HOMO (now a singly occupied molecular orbital-SOMO) resembles the HOMO shown in Figure S20 the orbital just below it in energy (HOMO-1) is two lone pairs localised on the distal oxygen of the anthraquinone-based ligand. The TD-DFT calculated absorption spectrum is dominated by a low-energy profile (*ca.* 830 nm) which has characteristic electron transitions of mixed ligand-to-metal charge transfer (LMCT) and $n-\pi^*$. Noting that the excited state property of $[\text{Ru}(\text{bipy})_3]^{2+}$ is governed by the triplet state a TD-DFT calculation was also performed on the T1 state of **RU1** for a comparison purpose (Figure S23). The structure for the T1 state shows a clear distortion at the anthraquinone-based ligand, very similar in appearance to the oxidised structure (Figure S22). The Ru-O2 bond length decreases by around 3% but the effect at Ru-O1 is less significant (< 1%); the average Ru-N bond length is 2.096 Å which is slightly greater than for the ground state (2.083 Å). There is no indication from the calculations that the anthraquinone-based ligand is more weakly bound to the ruthenium centre in the triplet excited state; it is the bipyridine ligands that are conceivably less tightly bound.

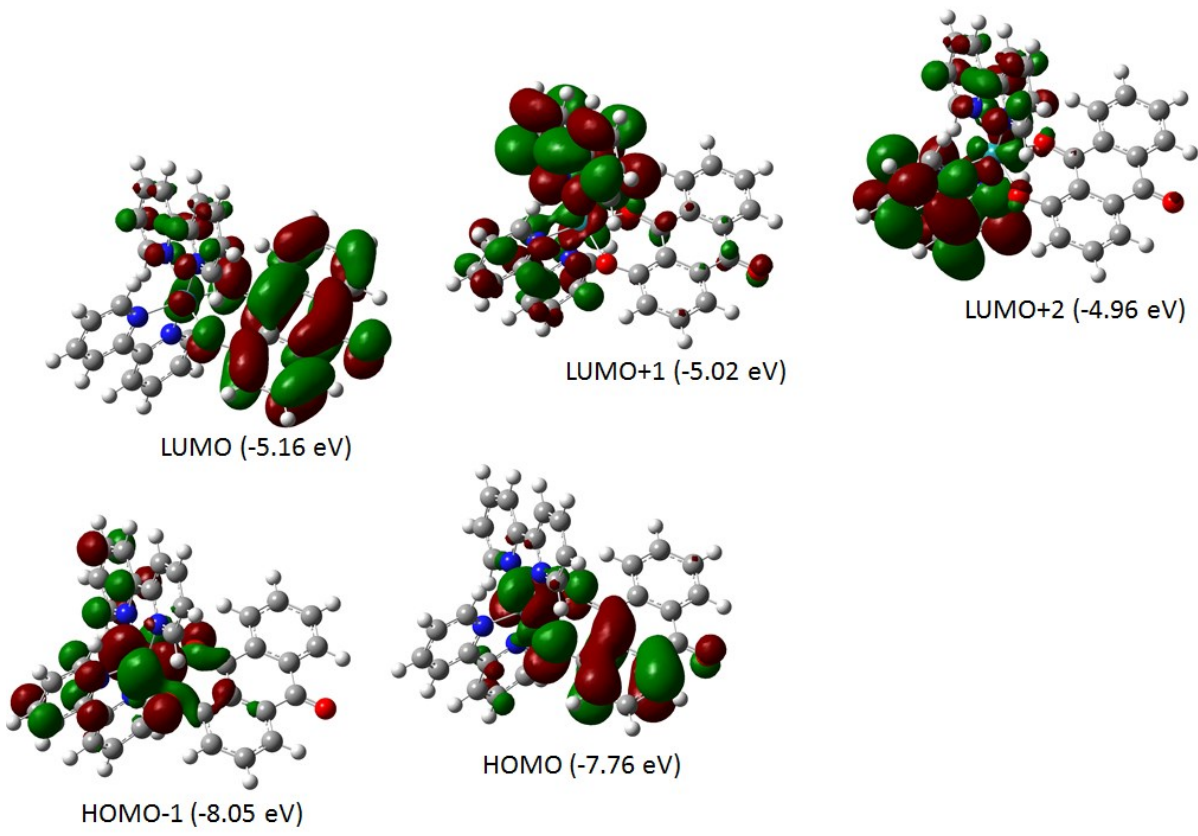


Figure S20. Selection of DFT calculated Kohn-Sham frontier molecular orbitals for a gas-phase energy minimised structure of **RU1** using Gaussian 09 and B3LYP with a split basis set with 3-21G* for Ru and 6-311G for all other atoms.

Table S2. Calculated parameters from TD-DFT for energy minimised structure of **RU1** in the gas phase using B3LYP and 3-21G* (Ru) and 6-311G (other atoms).

Wavelength / nm (oscillator strength)	Orbital Contribution ^a	a^2 ^b
619 (0.0134)	HOMO-1 to LUMO+1 HOMO to LUMO HOMO to LUMO+1 HOMO to LUMO+2	0.0173 0.1786 0.1205 0.1537
603 (0.0129)	HOMO-1 to LUMO+2 HOMO to LUMO HOMO to LUMO+1 HOMO to LUMO+2	0.0323 0.0619 0.3300 0.0439
594 (0.0129)	HOMO-1 to LUMO+2 HOMO to LUMO HOMO to LUMO+2	0.0443 0.2214 0.2084
582 (0.0043)	HOMO-1 to LUMO	0.4648
567 (0.0241)	HOMO-2 to LUMO+1 HOMO-1 to LUMO+1 HOMO-1 to LUMO+2 HOMO to LUMO	0.0215 0.4321 0.0176 0.0199
532 (0.0557)	HOMO-2 to LUMO+2 HOMO-1 to LUMO+1 HOMO-1 to LUMO+2 HOMO to LUMO+1 HOMO to LUMO+2	0.0655 0.0204 0.3180 0.0140 0.0585

^a Major orbital contribution to transition shown in bold. ^b molecular orbital coefficient squared.

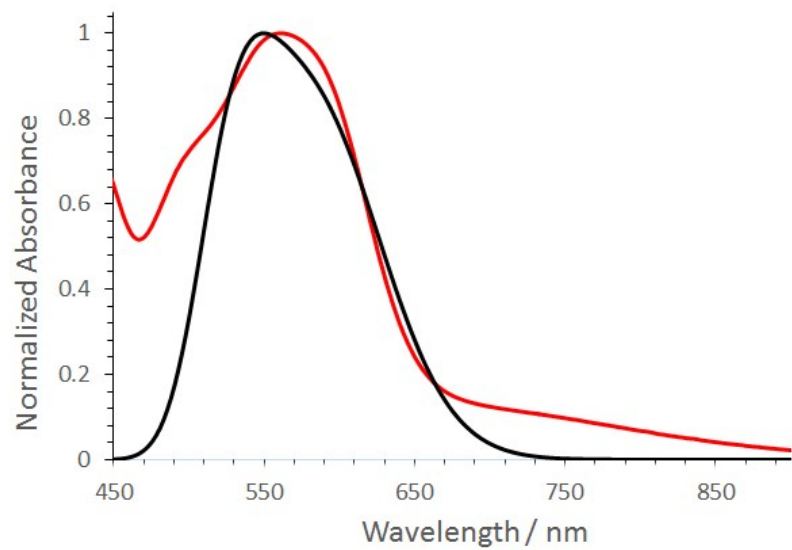


Figure S21. Comparison of recorded normalized absorption spectrum of **RU1** in MeCN (red) with calculated spectrum (black) for the energy minimized gas phase structure. The half-width for the calculated spectrum was set to 1100 cm^{-1} to match the actual spectrum.

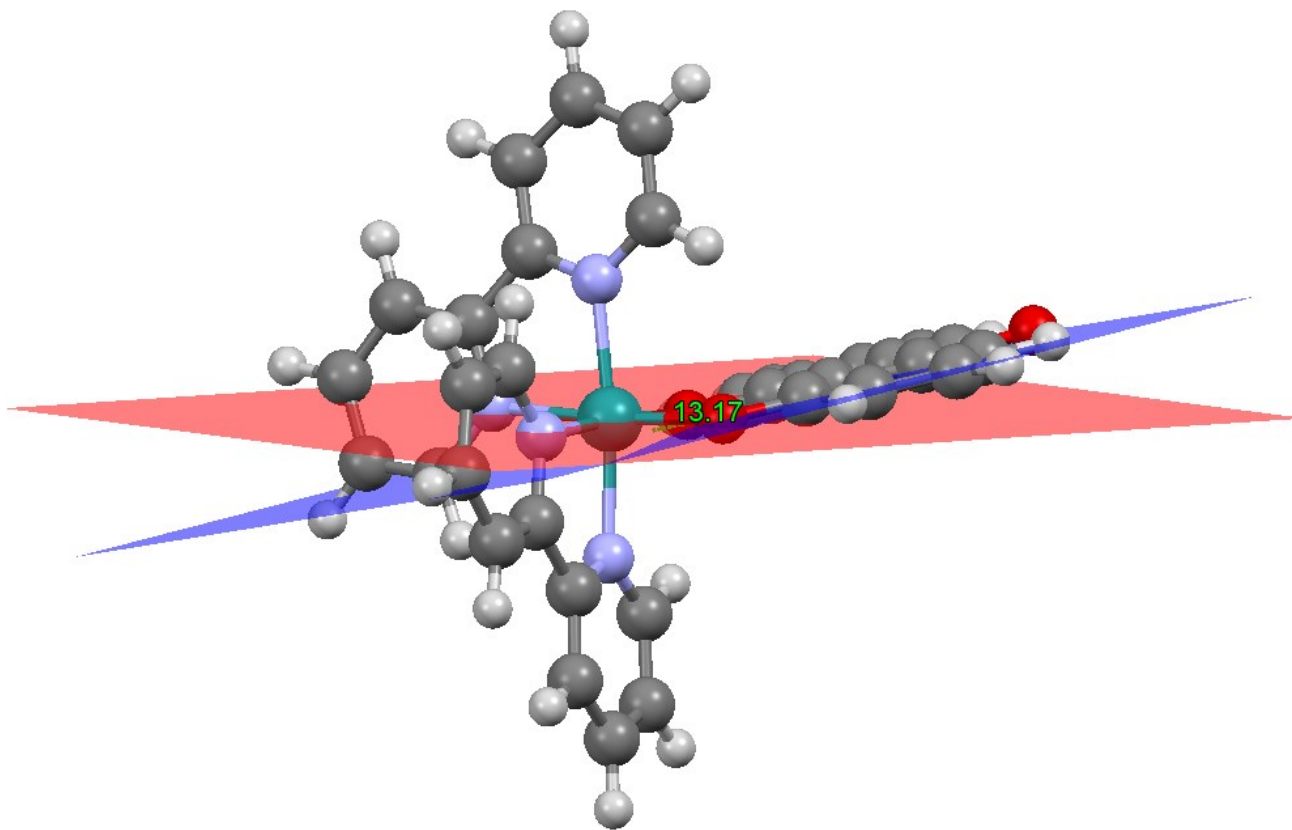


Figure S22. Calculated structure of $[\text{Ru}^{3+}(\text{bipy})_2\text{AQ}]^{2+}$ and the tilt angle between planes created using the RuN_2O_2 unit (red) and the anthraquinone-based ligand (blue).

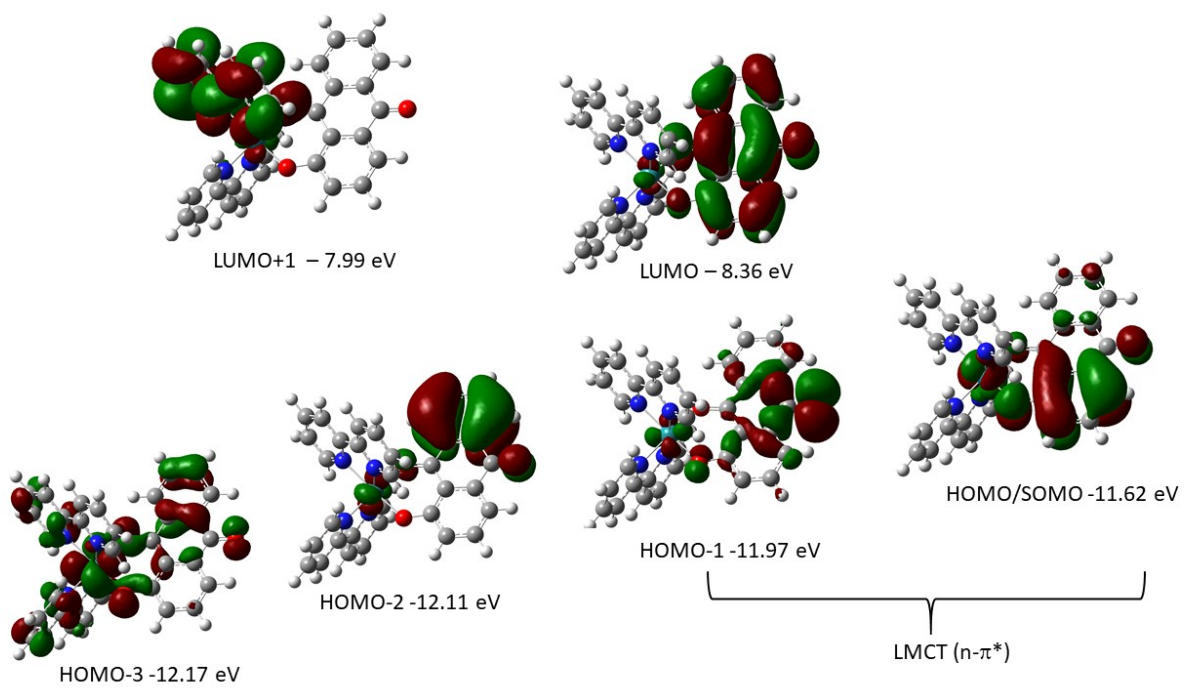


Figure S23. Selection of DFT calculated Kohn-Sham frontier molecular orbitals for a gas-phase energy minimised structure of $[\text{Ru(III)(bipy)}_2\text{AQ}]^{2+}$ using Gaussian 09 and B3LYP with a split basis set with 3-21G* for Ru and 6-311G for all other atoms.

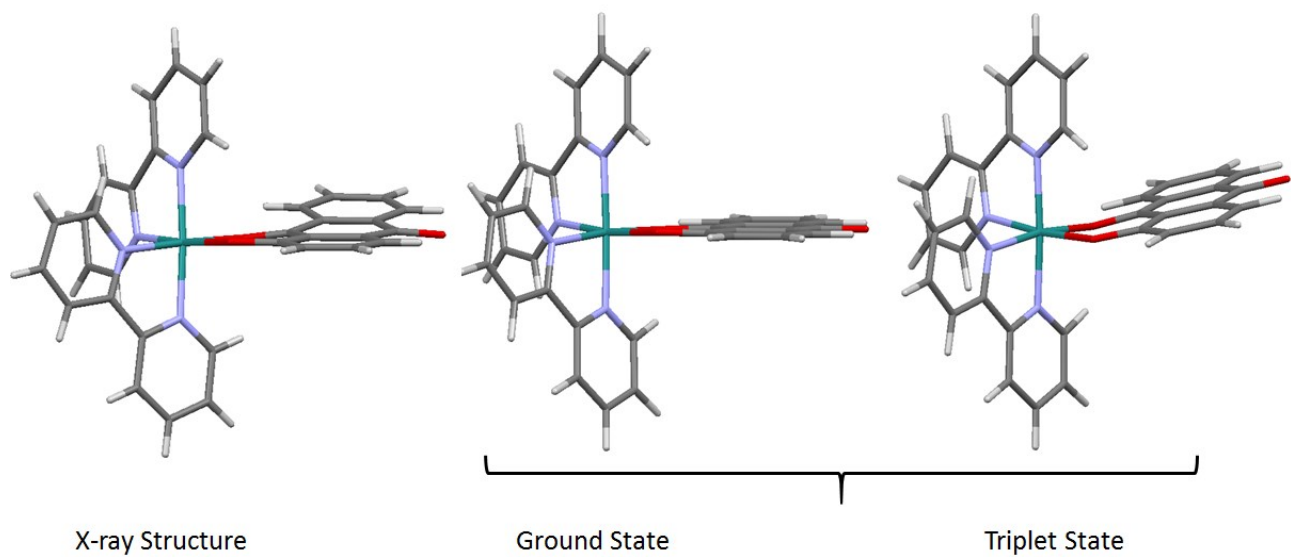


Figure S24. Comparison of X-ray structure for RU1 with calculated ground-state and first-excited triplet state structures.

References

1. E. A. Seddon and K. R. Seddon, *The Chemistry of Ruthenium*, Elsevier, 2013.